

Mechanical Characteristics and Failure Modes of Low-Strength Rock Samples with Dissimilar Fissure Dip Angles

Y L WANG^{a,b,1}, D S LIU^a, K LI^a, X M HU^c and D CHEN^d

^a *Chongqing Bureau of Geology and Minerals Exploration, Chongqing 401121, China*

^b *State Key Laboratory of Coal Mine Disaster Dynamics and Control, Chongqing University, Chongqing 400044, China*

^c *Chongqing Gaoxin Engineering Survey and Design Institute Ltd, Co., Chongqing 401121, China*

^d *Chongqing Vocational Institute of Engineering, Chongqing 402260, China*

Abstract. The mechanical characteristics and failure modes of low-strength rock sample with various fissure dip angles were investigated by conventional uniaxial compression test and three-dimensional (3D) crack reconstruction. The results indicated that compared with high-strength rock masses, cracks had different influences on the low-strength rock mass mechanical deformation features. Thereinto, the dip angle of fissures can cause post-peak failure stage of stress-strain curve change from swift decline to multi-step down, showing obvious ductility deformation and failure characteristics. Peak strength and elastic modulus owned an anti-S-shaped growth tendency with the growth of fissure dip angle, which was positively correlated and greatest subtle to the fissure dip angle $\alpha < 21^\circ$ and $\alpha > 66.5^\circ$. The axial peak strain reduced first and enlarged rapidly with growing fissure dip angle, suggesting a V-shaped change trend. Increasing the fissure dip angle will change the sample failure mode, experienced complete tensile failure to tensile-shear composite failure, and ultimately to typical shear failure. Also, the crack start angle decreased with enlarging fissure dip angle, larger than that the high-strength rock mass fissure dip angle. The above research findings can complement and improve the study of fissured rock masses.

Keywords. Low-strength specimen, pre-existing fissure, mechanical property, failure mode, 3D-crack reconstruction

1. Introduction

There exist substantial primary and structural fissures in engineering rock masses. The objects directly faced in geotechnical engineering are rock masses with certain structural characteristics, mainly composed of structural bodies (rock) and complex structural surfaces (joints, fissures, etc.) [1-3]. With the development of geotechnical investigation methods and further research on rock mechanics, people have gradually recognized that under the influence of geological environment and engineering disturbance, the expansion and interpenetration of fissures are the main failure modes of engineering rock

¹ Corresponding Author, Y L WANG, Chongqing Bureau of Geology and Minerals Exploration, Chongqing 401121, China; Email: 860024333@qq.com.

masses. Thus, it will be very imperative to learn the mechanical and deformation failure traits of fissured rock masses, and it also has engineering value for engineering excavation and stability analysis.

To comprehend fissured rock mass deformation and failure modes, considerable experimental studies have been correspondingly conducted. From Bombolakis [4] acquiring the failure properties of pre-fissured samples with uniaxial compression, many fissured rock experiments were explored to attain their deformation and strength behaviors. For instance, the scientists [5, 6] also researched strength and deformation attributes of pre-fissured marble in conservative uniaxial compression and triaxial compression. Moreover, complete and imperfect samples owned various deformation aspects with the peak stress, and the mode of peak strength and failure relied on fracture geometry and the confining pressure. Shen [7] researched fracture beginning in rock-like materials and described three kinds of material failure, including shear, tensile and mixed failures. Moreover, Wong and Einstein [8] summarized former literatures and concluded effects of fissure geometry (fissure angle, ligament length and angle) upon fracturing procedure and coalescence pattern of Carrara marble samples with two exposed cracks. Also, Yang and Jing [6] conducted uniaxial compression researches on a sand stone sample including a crack to learn impacts of single crack angle and length on the deformation and strength failure performance. Furthermore, based on two pre-existing transfixion fissures with triaxial compression, Xiao et al. [9] worked on the failure traits of marble, and determined that anti-wing cracks were chief form of cracks that influence the eventual failure mode of samples. These reports are that with uniaxial, biaxial or triaxial compression, concentrated on mechanical properties and crack propagation law of pre-fissured samples with single [10, 11], double [8, 12, 13] or multiple [14, 15] rectangular defects. Compared with uniaxial and biaxial compression tests, triaxial compression tests are rare, mainly because triaxial compression tests can simulate the real environment of the rock mass, but cannot directly observe the initiation and expansion of new cracks. Relative to uniaxial and biaxial compression tests, it is rarely seen triaxial compression tests, which tests can fake the practical surroundings of rock mass, but cannot straightly perceive new fissure initiation and expansion. Besides, the constituents applied to produce the pre-fissured specimens can be separated into two groups: rock-like and real rock materials. There exist numerous rock-like materials, e. g., glass, Columbia Resin 39, cement, molded gypsum, and various mixed materials [12, 16]. The real rock material are mainly high-hardness rock masses, such as granite [17], marble [18, 19], granodiorite [8, 20], limestone [21], sandstone [6]. Meanwhile, the methods of pre-existing cracks mostly contain laser, hydraulic, and blade cutting, and pre-buried fissure, etc. True rock samples are primarily processed by the first three means, and the rock-like material samples are commonly treated by pre-buried fissures. Usually, pre-buried fissures and blade cutting are applied based on production price and technical requirements of the specimens.

The above experiments have obtained abundant findings, which own vital guiding meaning for learning mechanical features, crack propagation principles and deformation instability characteristics of fissured rock masses. However, there still exist many deficiencies in relevant research at this stage, which can be summarized as follows:

- (1) Most experimental works were restricted to conservative compression tests on high-strength rock masses of pre-fissured samples, but the investigation of mechanical belongings and failure modes of low-strength rock examples with pre-existing cracks was still rare. In wildlife, rock masses with low strength frequently comprise extra major joints and fissures than rock masses with high strength, which can possibly generate

secondary fissure beginning and expansion, leading to the total unsteadiness and failure for the rock mass.

(2) Whether it was a conventional compression test or a numerical simulation test, the experimental conclusion was mostly based on the analysis of the two-dimensional image or the cutting face of the specimen during the test. Although the experimental results obtained had certain research significance, the original and secondary cracks in the rock specimen both initiated and expanded in three dimensions. The final failure of specimens was also the result of the interaction between cracks. Thus, the simple two-dimensional analysis cannot fully reflect the fissure start and propagation law and the final failure mode of samples.

Thus, it is critical to systematically explore the mechanical attributes and real three-dimensional failure mode of fissured rock masses with low strength. To more profoundly acquire strength, deformation, and crack coalescence patterns of rock samples with low strength, conventional uniaxial compression tests and three-dimensional (3D) crack reconstruction were performed on sandy mudstone rock-like material samples with dissimilar fissures geometries. The experimental results can further supplement and perfect the research in related fields of fissured rock masses and enrich its research methods.

2. Experimental Methodologies

2.1. Specimen Preparation

Low-strength rock masses can be established as UCS smaller than 30 MPa [22], and the sandy mudstone was chosen under the average value 28. 23 MPa of UCS, from a mine in Sichuan, China. It hardly created specific cracks in practical rocks. Thus, the study used rock-like materials to conduct experimental investigation in associated parts. The existed experiments suggested a strong similarity between mechanical parameters and other characteristics of rock-like or rock materials [16]. In other words, it is achievable to apply rock-like materials to substitute rock materials for exploring mechanical principles and failure modes.

From indoor matching trials, cement mortar with mass ratio for water: sand (80 mesh): cement (32. 5 grade) of 0. 4: 1. 0: 1. 0: was selected to form sandy mudstone rock-like materials. The basic physical and mechanical parameters of real sandy mudstone and rock-like materials are shown in table 1. Moreover, figure 1 suggests the uniaxial compression relationship between stress and strain and crack patterns of the complete rock-like specimens and sandy mudstone samples. From table 1 and figure 1, it can be seen that the failure modes and mechanical properties and of the two specimens are in good agreement, demonstrating the feasibility of using rock-like materials samples rather than sandy mudstone specimens for more investigation. The pre-present cracks were through-opened fissures, formed by pre-buried steel bars. According to the method proposed from the International Society of Rock Mechanics, the prepared specimens had cylindrical shape (diameter 50 mm× height 100 mm)100 mm. Figure 2 indicates numerous sorts of rock-like specimens exhaustively. The crack geometry of the pre-fractured sample can be determined: α is the fissure inclination angle, $2a$ and $2b$ are corresponding to the fissure length and width. Moreover, the pre-present cracks were positioned in the sample middle to minimalize influences of end friction on the experimented specimens.

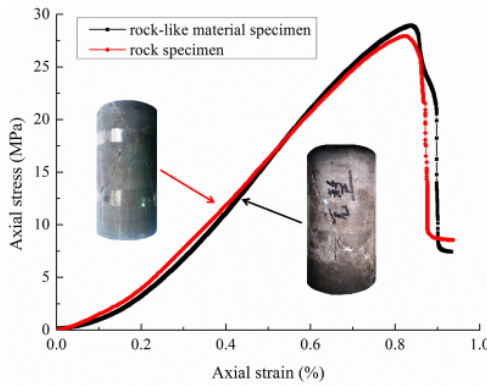


Figure 1. Uniaxial compression stress-strain relationship and failure modes of samples of sandy mudstone and rock-like materials.

Table 1. Basic parameters of rock-like material and sandy mudstone.

Type	Density P ($\text{g}\cdot\text{cm}^{-3}$)	UCS σ_c (MPa)	Tensile strength σ_t (MPa)	Elastic modulus E (GPa)	Poisson ratio ν	Cohesive force c (MPa)	Internal frictional angle φ ($^\circ$)
Sandy mudstone	2.42	28.23	2.54	7.25	0.22	22.68	31.8
Rock-like material	1.96	27.08	2.32	5.88	0.25	20.42	33.7

To study the impact of dissimilar geometric pre-present cracks on the mechanical properties and failure modes of sandy mudstone samples, one experimental scheme was schemed in the article: The single-cracked samples owned various inclination angles; $2a$ was 15 mm and $2b$ was 2 mm. α was equal to $0^\circ, 15^\circ, 30^\circ, 45^\circ, 60^\circ, 75^\circ$ and 90° . Table 2 indicates the detailed test scheme. To lower the dispersion of test outcomes, three pre-present fissure samples were made for each influence factor. Under the identical experimental circumstances, three parallel examinations were conducted to confirm the efficiency of the experiment. The standards followed: (1) The failure modes of samples should be principally same; (2) It should own a close stress-strain curve. Meanwhile, two specimens at least can satisfy the criteria, and if possible, additional samples can be employed for repeatability trying.

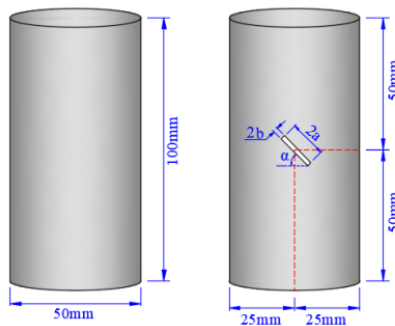


Figure 2. Dissimilar geometric pre-present cracks in rock-like material specimens.

Table 2. Strategy of examination scheme.

No.	Examination scheme	Geometric variable	Geometric invariant
I	Single-cracked sample with various dip angle	0°, 15°, 30°, 45°, 60°, 75°, 90°	2a = 15 mm, 2b=2 mm

2.2. Testing Procedure and Reconstruction Method

For MTS 815 rock mechanics servo control test systems, the complete and pre-fissured rock-like samples are subjected to conservative uniaxial compression examinations, and the maximum axial load capacity is 2800 KN. Experiments applied displacement-controlled quasi-static loading mode using a fixed rate of 0.002 mm/s till a failure happened. First, two short cylindrical rigid steel blocks with the equal diameter were located on both ends of the specimen as the experimented sample. Besides, applying a moderate petroleum jelly to the contact surface between the sample end and the steel block can expressively lower the impact of end friction on experimental outcomes. In the process of loading, the fissure start and expansion of sample were recorded using a high-definition camera for later analysis.

By combining CT scanning with Avizo software processing, 3D-crack reconstruction was performed. CT scanning technology has the advantages of lossless, dynamic, quantitative detection, and high-resolution digital image display. Also, Avizo software possesses the characteristics of 3D visualization and data direct output. First, a CT scan was conducted on the pre-fissured specimens after uniaxial compression test with the Micro XCT-400 test system. After that, Avizo 8. 0 software was used to process the scanned slices by median filtering, binary processing and finely processing in turn, as shown in figure 3. Finally, the processed 2D scanning slices were reconstructed to acquire 3D digital specimens. After crack extraction, a 3D-crack reconstruction model could be obtained. The detailed process is shown in figure 4.

3. Experimental Results

According to the uniaxial compression test and 3D-crack reconstruction results, this section analyzes the mechanical belongings and distortion failure features of low-strength pre-fissured specimens.

3.1. Strength and Deformation Properties

Figure 5 shows the stress-strain relationships of single-cracked samples with dissimilar crack dip angles. It is obviously that samples with larger dip angle fissures had greater peak strength (UCS) and larger peak strain. Besides, with growing fissure dip angle, the slope of stress-strain curve linearity range progressively increases, which indicates the elastic modulus increased based on increasing fissure dip angle. The above phenomenon was similar to those of high-strength specimens, but the low-strength specimens typically showed unique characteristics in post-peak stage. The main manifestation was from rapid drop (brittle failure characteristics) to multi-step drop (ductile failure characteristics). This transformation became more pronounced as the crack dip angle decreases, in particular for the case of smaller than 60°. All analyses indicate the mechanical belongings of single-fissured samples are intimately associated to the angle of the fissure dip.

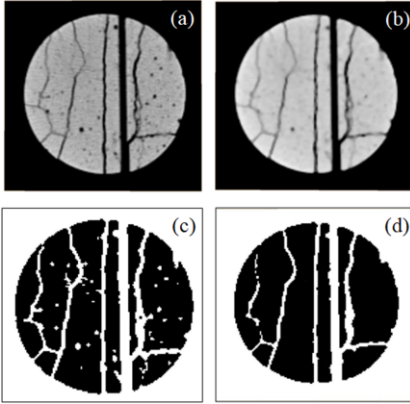


Figure 3. Processing of CT scanning diagram.

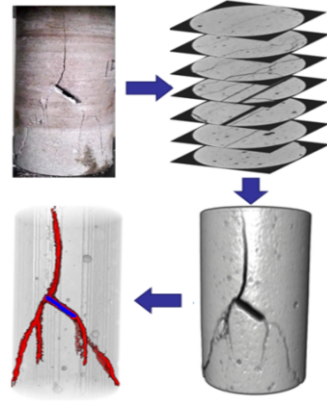


Figure 4. Process schematic diagram of 3D-crack reconstruction.

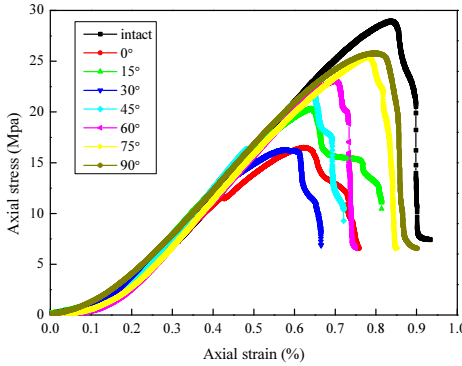


Figure 5. Stress and strain relationship of single-fissured samples with dissimilar crack dip angles.

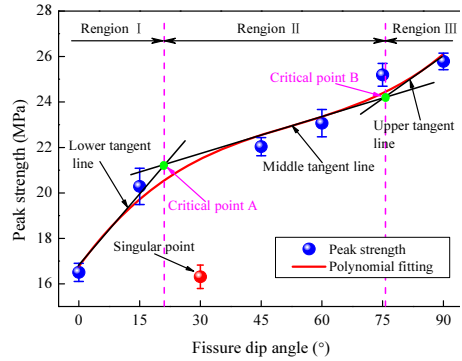


Figure 6. Peak strength vs. fissure dip angle.

To better understand the connection between peak strength and fissure dip angle, a further specific and quantitative exploration of influence of fissure dip angle on peak strength, which can be found in figure 6.

Figure 6 demonstrates the alteration of the peak strength of single-cracked samples with fissure dip angles, suggesting a cumulative tendency of "drastic – gentle – drastic". Yet, there existed a deceptive singular point at which the fissure dip angle was equal to 30°. The probable reason was that if $\alpha = 30^\circ$, the difference between the fissure dip angle and internal friction angle of specimen was smallest. The polynomial fitting curve presented a slant anti-S shape without considering the singularities. Points A and B were the critical points of polynomial fitting curve, established as intersection of the middle tangent line and lower (upper) tangent line of fitting curve. Two-point horizontal coordinates were corresponding to 21° and 76°. Thus, the curve can be separated as the following three regions:

Region I ($\alpha < 21^\circ$)

In this region, with growing fissure dip angle, peak strength exhibited a sharp increasing tendency, meaning this strength was very subtle to fissure dip angle.

Region II ($21^\circ < \alpha < 76^\circ$)

At this stage, the peak strength increased slowly with increasing fissure dip angle. This suggested if $21^\circ < \alpha < 76^\circ$, this strength was unresponsive to the enlargement of fissure dip angle.

Region III ($\alpha > 76^\circ$)

The peak strength in this area reverted to rapid growth trend, but the growth rate was lower than that of in region I. This demonstrates the strength was also easily changed by fissure dip angle.

To acquire the impact of fissure dip angle on the distortion performance of single-fissured samples, the relationship between elastic modulus, peak strain or fissure dip angle were explored, as shown in figures 7 and 8.

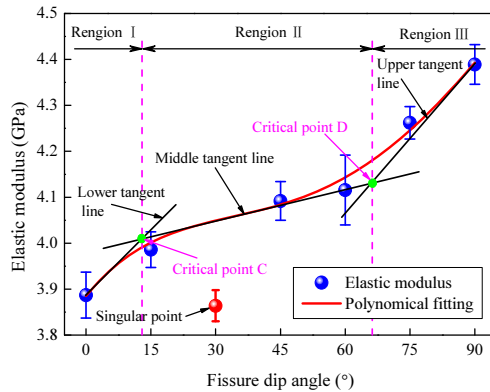


Figure 7. Elastic modulus vs. fissure dip angle.

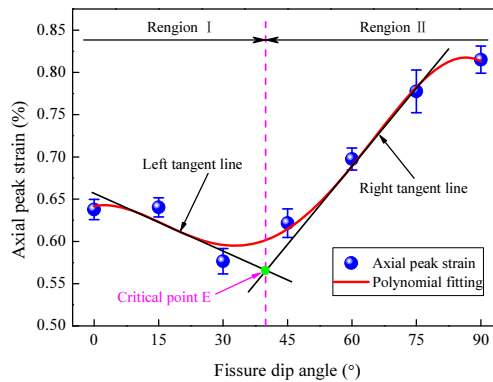


Figure 8. Relationship between the axial peak strain and fissure dip angle.

From figure 7, the variation law of elastic modulus with fissure dip angle was close to that of the peak strength, and also demonstrated a cumulative tendency of “drastic-gentle-drastic”. There was also a singular point ($\alpha = 30^\circ$). When the singularity was not considered, a polynomial fitting equation can also be used to determine the relationship between elastic modulus and fissure dip angle. Points C and D depicted in figure 7 were the vital points of the fitted curve, and the corresponding horizontal coordinates were 13.0° and 66.5° . According to the two points, the polynomial fitting curve of elastic modulus can be similarly categorized into the following three portions:

Region I ($\alpha < 13.0^\circ$)

The elastic modulus increased greatly with growing fissure dip angle, suggesting that the fissure dip angle influence on elastic modulus was large.

Region II ($13.0^\circ < \alpha < 66.5^\circ$)

In this region, the elastic modulus also increased with increasing of dip angle, but the increasing range was small.

Region III ($\alpha > 66.5^\circ$)

While the fissure dip angle located in the region III, the elastic modulus can be easily altered by enhancing fissure dip angle. This suggests that the enlargement of fissure dip angle meaningfully strengthened the sample ability to struggle axial twist.

Figure 8 plots the relationship between axial peak strain and crack dip angle is plotted in. Obviously, as the fissure dip angle increased, the axial peak strain decreased first and then increased rapidly. The critical point E can be determined after polynomial fitting, with the horizontal coordinate of 38.0° . According to the vital point, the polynomial fitting curve of the axial peak strain can also be divided into two parts:

Region I ($\alpha < 38.0^\circ$)

The axial peak strain gradually decreased if fissure dip angle enhanced, but this decreasing degree was very small. Overall, the impact of crack dip angle on axial peak strain was not very apparent in this region.

Region II ($\alpha > 38.0^\circ$)

In this region, the axial peak strain increased rapidly with enlarging fissure dip angle, demonstrating that axial peak strain was strongly impacted by the fissure dip angle. In addition, it shows that the fissure dip angle growth can strengthen the capacity of cracked samples to withstand axial strain at points correlated to peak strength.

To sum up, the crack dip angle owned a large effect on the strength and distortion properties of fissured specimens. However, this influence degree of crack dip angle in different ranges was very different.

3.2. Crack Propagation and Failure Modes

3D-crack reconstruction was completed for the intact and single-fissured specimens after fracture. The results can more directly and comprehensively reflect the crack propagation inside the specimen, as shown in figure 9.

In figure 9a, an oblique through crack was formed inside the intact specimen, which represented a characteristic single-slope shear failure. From figure 9b, the failure of 0° fissured sample was caused by multiple tensile cracks in the middle and both ends of the pre-fissure spreading upward and downward to the boundary, behavior as a typical tensile failure. Figure 9c exhibits the tensile fissures at both ends of 15° pre-fissure spread to boundary, resulting in specimen failure. Moreover, there was a branch shear fissure in the bottom of sample. Overall, tensile failure was the main reason and shear failure locally existed. Figure 9d shows the final crack propagating pattern of the 30° fissured specimen. Thus, three tensile fissures and two shear fissures extending from the pre-fissure caused the tensile-shear composite failure of the specimen. It can be concluded from figures 9e and 9f that the crack-propagating patterns of the 45° and 60° fissured specimens were basically the same, and they were the typical tensile-shear composite failure modes generated by tensile and shear fissures extending from both ends of the pre-fissure to upper and lower boundaries. From figure 9g, shear fissures produced at the end of the pre-fissure gradually changed into a tensile crack and extended to the boundary during the extension process, causing the 75° fissured specimen to break. In general, the

shear failure was primary, and the tensile failure was secondary. The 90° fissured sample in figure 9h was a typical single-slope shear failure similar to intact specimen. The inclined shear crack passed through the pre-fissure and extended to the boundary of the specimen.

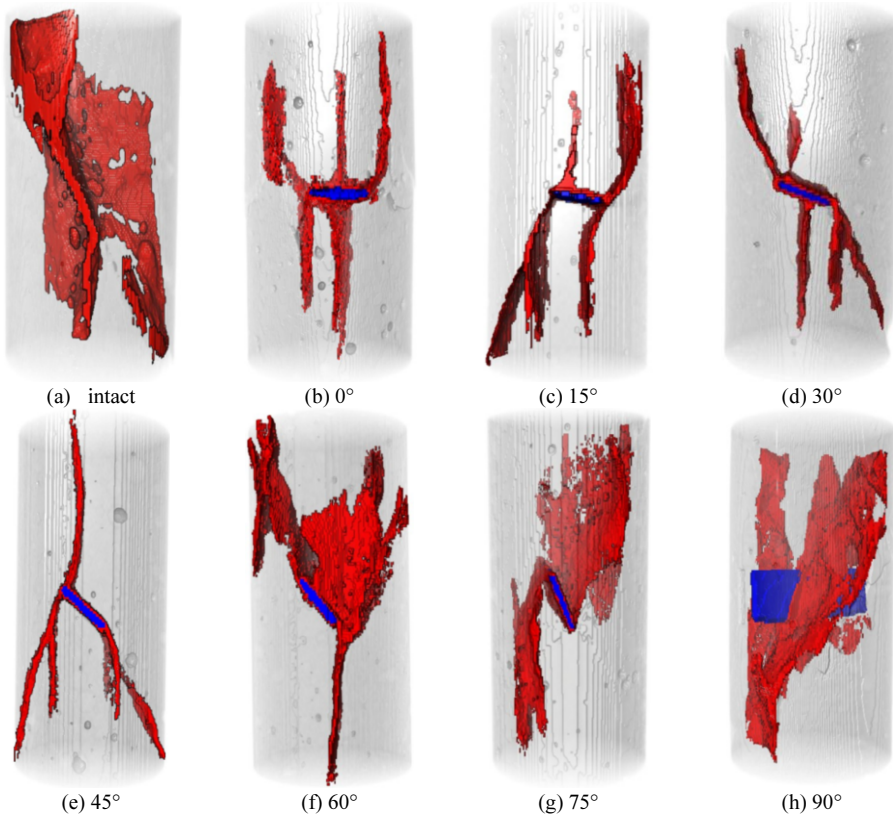


Figure 9. Crack propagation diagram of single-cracked samples with various crack dip angles (The gray shadow part is a specimen body, the blue part is a pre-fissure, the red part is a propagating crack).

The above analysis shows that the existence of pre-fissure had a large impact on the start and expansion of internal fissures in the samples, and can entirely alter its failure pattern. Meanwhile, the degree of impact was closely related to the crack dip angle, and the influence of smaller dip angle fissure was often larger. When the crack dip angle augmented to 90° , this influence was minimal. The sample failure pattern altered with fissure dip angle (from 0° to 90°), as shown below: typical tensile failure \rightarrow main tensile and secondary shear failure \rightarrow tensile-shear composite failure \rightarrow main shear and secondary tensile failure \rightarrow typical shear failure.

4. Conclusion

(1) In this paper, through uniaxial compression test and 3D-crack reconstruction technology, the mechanical possessions and failure modes of low-strength rock samples

having dissimilar fissure dip angles were systematically studied. The results show that the crack inclination angle owned different degrees of degradation effects on the elastic modulus, stress-strain curve, peak strength strain, and can affect or even change the extended shape and type of cracks in the specimen.

(2) Crack inclination angle can significantly impact the stress-strain curve, especially the post-peak failure stage. Thereinto, the crack inclination angle can change the stress-strain curve from swift decline to multi-step down, showing obvious ductile damage characteristics.

(3) The peak strength and elastic modulus exhibited an anti-S-shaped growth tendency as the inclination of the crack increased, and were most influenced by small inclination angle crack ($\alpha < 21^\circ$) and the large dip angle fissure ($\alpha > 66.5^\circ$). The axial peak strain slightly decreased first and then rapidly increased with the increase of fissure dip angle (the demarcation point was 38°).

(4) With the inclination of the crack increased, failure modes of specimen altered from complete tensile to tensile-shear composite failure, and finally became typical shear failure. In addition, the fissure beginning angle declined with increasing fissure dip angle, from 71° and 90° , which was larger than that of the high-strength rock mass.

Acknowledgements

This work was supported by the Chongqing Natural Science Foundation Project (Postdoctoral Science Foundation) (cstc2020jcyj-bsh0137) and Scientific research project of Chongqing Bureau of Geology and Minerals Exploration (DKJ-2020DZJ-A-015).

References

- [1] Janeiro R P and Einstein H H 2010 Experimental study of the cracking behavior of specimens containing inclusions (under uniaxial compression) *International Journal of Fracture* **164** (1) 83-102.
- [2] Huang D, et al. 2016 Investigation on mechanical behaviors of sandstone with two preexisting flaws under triaxial compression *Rock Mechanics and Rock Engineering* **49** (2) 375-399.
- [3] Park C H and Bobet A 2009 Crack coalescence in specimens with open and closed flaws: A comparison *International Journal of Rock Mechanics and Mining Sciences* **46** (5) 819-829.
- [4] Bombolakis E G 1968 Photoelastic study of initial stages of brittle fracture in compression *Tectonophysics* **6** (6) 461-473.
- [5] Yang S Q, et al. 2009 Experimental study on mechanical behavior of brittle marble samples containing different flaws under uniaxial compression *Engineering Fracture Mechanics* **76** (12) 1833-1845.
- [6] Yang S Q and Jing H W 2011 Strength failure and crack coalescence behavior of brittle sandstone samples containing a single fissure under uniaxial compression *International Journal of Fracture* **168** (2) 227-250.
- [7] Shen B 1995 The mechanism of fracture coalescence in compression-experimental-study and numerical-simulation *Engineering Fracture Mechanics* **51** (1) 73-85.
- [8] Wong L N Y and Einstein H H 2009 Einstein, Crack coalescence in molded gypsum and carrara marble: part 2—microscopic observations and interpretation *Rock Mechanics and Rock Engineering* **42** (3) 513-545.
- [9] Xiao T, Li X and Jia S 2015 Failure characteristics of rock with two pre-existing transfixion cracks under triaxial compression *Yanshilixue Yu Gongcheng Xuebao/Chinese Journal of Rock Mechanics and Engineering* **34** (12) 2455-2462.
- [10] Manouchehrian A, et al. 2014 A bonded particle model for analysis of the flaw orientation effect on crack propagation mechanism in brittle materials under compression *Archives of Civil and Mechanical Engineering* **14** (1) 40-52.
- [11] Renshaw C E and Schulson E M 2001 Universal behaviour in compressive failure of brittle materials

Nature **412** (6850) 897-900.

- [12] Lee H and Jeon S 2011 An experimental and numerical study of fracture coalescence in pre-fissured specimens under uniaxial compression *International Journal of Solids and Structures* **48** (6) 979-999.
- [13] Li H Q and Wong L N Y 2014 Numerical study on coalescence of pre-existing flaw pairs in rock-like material *Rock Mechanics and Rock Engineering* **47** (6) 2087-2105.
- [14] Chen X, Liao Z and Peng X 2012 Deformability characteristics of jointed rock masses under uniaxial compression *International Journal of Mining Science and Technology* **22** (2).
- [15] Wong R H C, et al. 2002 Splitting failure in brittle rocks containing pre-existing flaws under uniaxial compression *Engineering Fracture Mechanics* **69** (17) 1853-1871.
- [16] Zhuang X Y, Chun J W and Zhu H H 2014 A comparative study on unfilled and filled crack propagation for rock-like brittle material *Theoretical and Applied Fracture Mechanics* **72** 110-120.
- [17] Isaka B L A, et al. 2018 An influence of thermally-induced micro-cracking under cooling treatments: mechanical characteristics of Australian granite *Energies* **11** (6).
- [18] Li Y P, Chen L Z and Wang Y H 2005 Experimental research on pre-fissured marble under compression. *International Journal of Solids and Structures* **42**(9-10) 2505-2516.
- [19] Yang S Q, et al. 2008 Experimental investigation on strength and failure behavior of pre-fissured marble under conventional triaxial compression *International Journal of Solids and Structures* **45** (17) 4796-4819.
- [20] Wong L N Y and Einstein H H 2009 Crack coalescence in molded gypsum and carrara marble: Part 1. macroscopic observations and interpretation *Rock Mechanics and Rock Engineering* **42** (3) 475-511.
- [21] Rinehart A J, Bishop J E and Dewers T 2015 Fracture propagation in Indiana Limestone interpreted via linear softening cohesive fracture model *Journal of Geophysical Research-Solid Earth* **120** (4) 2292-2308.
- [22] Wang Y L, et al. 2018 Experimental study on mechanical properties and failure modes of low-strength rock samples containing different fissures under uniaxial compression *Engineering Fracture Mechanics* **197** 1-20.